Journal of Membrane Science 744 (2026) 125178

Contents lists available at ScienceDirect

Journal of Membrane Science

journal homepage: www.elsevier.com/locate/memsci

Nanofiltration of synthetic HTL-AP: rejection, fouling analysis, and membrane autopsy

Soorena Gharibian [a,*], Knud Villy Christensen [a], Rime Bahij [a], Morten Enggrob Simonsen [b], Massimiliano Errico [a,c]

[a] Chemical Engineering Section, Department of Green Technology, Faculty of Engineering, University of Southern Denmark, Campusvej 55, 5230, Odense, Denmark
[b] Department of Chemistry and Bioscience, Aalborg University, Niels Bohrs Vej 8, 6700, Esbjerg, Denmark
[c] Department of Mechanical, Chemical and Materials Engineering, University of Cagliari, Via Marengo 2, Cagliari, 09123, Italy

ARTICLE INFO

Keywords:
Biocrude
HTL
HTL-AP
Wastewater treatment
Nanofiltration: NF90

ABSTRACT

Valorization or recycling of the hydrothermal liquefaction aqueous phase (HTL-AP) pose a substantial obstacle to the commercial use of the HTL process for biomass (especially algal). This is due to its high concentration of organic constituents and nutrients. This article focus on nanofiltration (NF) of acidic and basic synthetic HTL-AP using a DuPont FilmTec™ NF90 membrane in a batch crossflow module. The emphasis is on rejection performance and fouling behavior, supported by membrane autopsy. Overall, almost 90 % rejection of COD, NH_4^+, and PO_4^{3-}, and TDS/conductivity was achieved. HTL-AP(pH = 4) led to higher NH_4^+ rejection (94 ± 1 %) compared with pH = 8.5 (83 ± 3 %). This can be attributed to the formation of a gel layer and the equilibrium between NH_4^+ and NH_3, favoring the more permeable NH_3 at higher pH. Flux monitoring revealed that NF90 performs better ($J_{30\ wt\%\ recovery}/J_0$ ca. 0.77 ± 0.02) with HTL-AP(pH = 8.5) than at pH = 4 (0.56 ± 0.06) since at pH = 8.5 most of the small organic compounds are deprotonated and therefore exhibit weaker interactions with the negatively charged NF90 surface. At both HTL-AP pH levels irreversible fouling is negligible while gel layer and concentration polarization are major contributors which are reversible through water flushing. Resistance due to the gel layer formation was more prominent for HTL-AP(pH = 4). The presence of a thin gel layer was confirmed through attenuated total reflectance-Fourier transform infrared spectroscopy (ATR-FTIR), scanning electron microscopy (SEM), water contact angle measurements, and thermal gravimetric analysis (TGA). In addition, fouling resistance due to pore blockage and persistent adsorbed foulants inside the membrane matrix is also a significant contributor. This was removed successfully by basic cleaning (NaOH).

1. Introduction

Renewable energy technologies are promoted as pathways to lessen reliance on conventional fossil fuels and to mitigate environmental issues associated with the use of fossil fuels including climate change. Yet, their widespread deployment is constrained by factors such as fluctuating energy output, significant upfront investment, and considerable land and water demands. In this context, producing biocrude from biomass stands out as a promising option, offering a renewable and potentially scalable energy resource [1]. Notably, hydrothermal liquefaction (HTL) has emerged as a highly effective method for transforming biomass into biocrude [2,3]. In contrast to carbonization and pyrolysis, HTL eliminates the need for energy-demanding dewatering or drying steps when processing wet biomass [1]. This characteristic makes HTL especially well-suited for algae which inherently has a high moisture content [4]. Algal feedstocks for HTL are commonly cultivated using urban wastewater as a nutrient source [5]. If HTL wastewater can be cleaned to a level where it resembles urban wastewater, it could be recycled and improve the process overall viability. Despite these benefits, HTL still faces notable challenges, especially concerning the by-products generated including the hydrothermal liquefaction aqueous phase (HTL-AP). HTL-AP is rich in heteroatom-containing organic compounds that create significant obstacles for HTL-AP reuse and disposal [1,5–8]. This hinders the development of a fully closed-loop process, thereby constraining the commercial economic viability and environmental sustainability of HTL.

To overcome these limitations, several valorization approaches for HTL-AP have been explored. These strategies involve recovering

* Corresponding author.
E-mail address: sog@igt.sdu.dk (S. Gharibian).

https://doi.org/10.1016/j.memsci.2026.125178
Received 6 December 2025; Received in revised form 10 January 2026; Accepted 19 January 2026
Available online 22 January 2026

valuable compounds, including platform chemicals and struvite [3,8], or converting it into H_2 and CH_4 through processes such as anaerobic digestion (AD) [1] or hydrothermal gasification (HTG) [9]. Another strategy is to reuse HTL-AP directly, either as the reaction medium in subsequent HTL runs or as a nutrient source for cultivating algal feedstock [4]. However, the contaminants present in HTL-AP can suppress algal growth, and repeated reuse leads to their buildup, which further amplifies these inhibitory effects [8,10]. This creates a need for robust separation and detoxification methods to ensure that HTL-AP can be reused safely and efficiently.

Among the various proposed solutions, membrane filtration cascades have attracted interest due to their capacity to selectively remove contaminants from HTL-AP [11,12]. These technologies can effectively remove organic inhibitors, heavy metals, and other unwanted constituents, thereby improving the suitable reuse of HTL-AP [13]. Membrane-based processes can also concentrate the nutrient content of HTL-AP, improving its potential for use as a growth medium in algal cultivation [6,14]. However, as reported by Gharibian et al. [15] there are only few studies on the application of membrane-based processes for the treatment and valorization of HTL-AP.

Zhang et al. [14] investigated nanofiltration (NF) of real HTL-AP (pH = 4.5) generated from swine manure and algae biomass. The real HTL-AP from different tests was accumulated and stored in drums for about six months. HTL-AP conductivity was 7.83 mS/cm. It contained significant concentrations of dissolved organic carbon (DOC, 11064 mg/L) and total phenols (2384 mg/L), composed largely of short-chain carboxylic acids (45 % of total organic carbon), phenolics, ketones, and aldehydes. Prior to NF using DuPont FilmTec™ NF90 at a transmembrane pressure (TMP) of 400 psi, several pretreatment methods were applied to HTL-AP to mitigate membrane fouling. pH adjustment using NaOH, thermal treatment, adsorption using granular activated carbon (GAC), and raw coal were investigated. In addition, pre/treatment by dead-end ultrafiltration (UF) using polyethersulfone (PES) membranes (with molecular weight cut off (MWCO) of 10000, 5000, and 1000 Da) was studied. The NF flux for HTL-AP(pH = 8) pre-treated by coal adsorption declined from an initial value of 43–53 to approximately 5 L/m^2.h as feed recovery increased to 80 wt%. DOC rejection averaged 74 %, with organic carbon mass recovery reaching up to 62 % at an 85 % feed recovery. NF fouling was due to the presence of humic-like compounds. The results suggest that integrating secondary separation processes can enhance the recovery and valorization of dissolved carbon in HTL-AP by recycling the NF concentrate back to the HTL feed slurry. In a recent study, Costa et al. [5] explored the use of NF (CR100, XLE, BW30 by DuPont FilmTec™) to treat HTL-AP (TMP = 400 psi). Three algal sources, including wastewater-grown algae (pH = 8.7) and harmful algal blooms (pH = 5.5 and 4.6), were used as the source of HTL-AP. Up to 99 % of organics were recovered in the NF retentate. Increasing the feed temperature to 45 °C and pH to 11 improved permeate flux and nitrogen compound separation. Recirculating the concentrated HTL-AP (NF reject) boosted biocrude yield, reduced nitrogen content by up to 12 %, and enhanced carbon and energy recovery by 66 % and 68 %, respectively. Overall, NF effectively reduced HTL-AP volume (35 wt% concentration factor) and strength while improving both yield and quality of biocrude. In a similar research, Szkadłubowicz et al. [16] investigated the treatment of post-processing liquid from the hydrothermal carbonization of sewage sludge (HTCL, pH = 7) using a combination of struvite precipitation and membrane filtration (microfiltration (MF), UF, and NF). Three ceramic and eleven polymeric membranes were tested to evaluate their performance on both the original HTCL and the liquid obtained after struvite precipitation (HTCLS, pH = 8.9). The results showed that membrane type and MWCO significantly affected permeate quality, with lower MWCO achieving greater rejection but also more fouling. For HTCL, the NPO30P NF membrane achieved the best performance, reducing NH_4^+ and nitrogen compounds by 24.4 and 22 %, respectively, while for HTCLS, the PES 5 kDa membrane provided the highest reductions (68.8 % for NH_4^+ and 52 % for nitrogen compounds). Implementing struvite precipitation prior to filtration enhanced the removal of chemical oxygen demand (COD, 12–63 %), total nitrogen (N_{total}, 31–70 %), and phosphate-phosphorus (PO_4–P, 51–81 %). It simultaneously improved membrane permeability by lowering fouling. In a practical study by Zhang et al. [12], the use of a dead-end NF process using DuPont FilmTec™ NF90 membrane to treat synthetic HTL-AP (pH = 2.6, as-is), with a focus on recovering carboxylic acids, was explored. The synthetic HTL-AP did not contain inorganic pollutants. Synthetic HTL-AP wastewater was created using compounds like acetic acid, propionic acid, isobutyric acid, etc. The NF experiments were conducted under acidic (pH = 2.6, as-is) and alkaline conditions (pH = 8, 9, and 10). 82.5 % DOC rejection under alkaline conditions (pH = 8), and up to 95 % rejection of isobutyric acid was achieved. Permeate flux under acidic conditions (pH = 2.6, as-is) ranged from 140 to 160 L/m^2.h, while alkaline conditions (pH = 8) showed reduced flux due to increased osmotic pressure. Rejections varied with pH; for example, the rejection of acetic acid reached 75 % at pH = 8, driven by charge exclusion rather than size exclusion alone. Recently, Sayegh et al. [17] examined oil and particles removal from HTL-AP (pH = 9) generated from municipal sewage sludge biomass. UF treatment of HTL-AP was performed using ceramic membranes (TiO_2, Inopor, Germany) in crossflow mode. The 10 nm pore size membrane had the most stable performance, achieving a critical flux of 6.6 L/m^2 h bar at 25 °C and maintaining a permeability around 18 L/m^2 h bar. The 5 nm membrane suffered significant fouling, particularly from surfactant adsorption. Separation of oil emulsions was effective, with a 90 % rejection of long-chain fatty acids and significant retention of anionic surfactants (85–90 %). However, total organic carbon (TOC) rejection was 3, 6, and 15 % for 30, 10, and 5 nm pore sizes, respectively, This is due to the presence of low MW organics such as short-chain fatty acids (e.g., hexanoic acid) and cyclic compounds (e.g., 2-piperidone) in the HTL-AP that can pass the UF membrane. Although the effect of different cleaning methods was studied and it shed light on the fouling mechanism to some extent, a detailed membrane autopsy was not covered.

According to the few available studies on the treatment of HTL-AP using membrane processes, UF can remove only large oil micelles and droplets, but not small organic molecules and salts/ions. Reverse Osmosis (RO) can remove monovalent ions and will strip HTL-AP of nutrients that would be necessary for the growth of microalgae if the aim is to reuse the treated HTL-AP as algae growth medium. In addition, most studies lack detailed fouling mechanism evaluation and do not incorporate membrane autopsy. Moreover, the use of synthetic wastewater is a common strategy in wastewater treatment research to evaluate process performance and investigate underlying mechanisms under controlled conditions. In the context of HTL-AP, many studies focused on separation processes have either built costly HTL setups or relied on aged samples collected/unified from several HTL runs [5,14], highlighting a gap in the development of synthetic HTL-AP, which would shift the attention to the treatment process rather than the HTL-AP generation process. Therefore, building on the few available studies and the potential of membrane-based processes for the treatment/valorization of HTL-AP, the present study evaluates NF process performance for the treatment of a complex synthetic HTL-AP containing both organic and inorganic pollutants. DuPont FilmTec™ NF90, a thin film composite (TFC) polyamide membrane, was selected based on its proven ability to remove small pollutants such as NH_4^+ [18,19] (ca. 90 % rejection) at a significantly lower operating pressure than RO [20]. Compared to earlier studies the current study takes multiple new aspects into account including: i) introducing a complex synthetic HTL-AP model wastewater to represent inorganic ions, organic pollutants spanning a broad molecular-weight range, and surfactants found in real HTL-AP, ii) rejection performance evaluation of DuPont FilmTec™ NF90 using a more realistic matrix of complex synthetic HTL-AP under slightly acidic and basic pH conditions, and iii) detailed membrane fouling behavior monitoring and identification of the underlying fouling mechanisms at two different pH conditions, supported by membrane

autopsy analysis. The results provide fruitful insights for future extended studies, especially for the treatment of real HTL-AP with a more complex wastewater matrix, by unraveling the complex operating/fouling mechanism of the NF process and improving the operation of multistage membrane-based systems for facile treatment/valorization of HTL-AP with low biodegradability and high toxicity. Moreover, synthetic HTL-AP is a high-strength model wastewater with a complex mixture of organic compounds, including those derived from lipid and oil fractions of biomass. This potentially makes it a model wastewater for NF treatment mimicking the behavior of oily wastewaters, thus providing broadly relevant insights for treating oily wastewater containing water-soluble organics, low amounts of emulsified oils, micelles, and mixed organic/inorganic pollutants.

2. Materials and methods

Deionized (DI) water (conductivity: <1 μS/cm) from a PURELAB Chorus 1 system (ELGA LabWater, Veolia Water Technologies, France) was used in all experiments. NaOH, $MgSO_4$, cyclopentanone (≥99 %), methylpyrazine (≥99 %), 3-hydroxypyridine (98 %), levulinic acid (98 %), and $(NH_4)_2HPO_4$ (≥98 %) were bought from Sigma-Aldrich (Germany). Acetic acid (99.9 %) was purchased from VWR (Denmark). NH_4NO_3, diiodomethane, and succinic acid (≥99 %) were purchased from Merck (Germany). Oleic acid (≥85 %) was purchased from TCI (Japan).

2.1. Synthetic HTL-AP

Organic constituents of synthetic HTL-AP were selected based on the study by Madsen et al. [21]. The detailed rationale is presented in the Supplementary Information file, section 1. Moreover, the concentration of NH_4^+ and PO_4^{3-} was selected based on the literature [1,22]. Tween-80, a non-ionic surfactant, was selected to create a homogenous single-phase solution similar to real HTL-AP. The presence of different surfactants in HTL-AP has been confirmed in previous studies [17,23]. Composition and general information about the synthetic HTL-AP are listed in Table 1. Two pH values of 4 and 8.5 were selected based on the literature [1,22] to cover both acidic and basic HTL-AP and different pH values reported in the literature. Initial/unadjusted pH level of the stock solution was 4 (as-is) while, pH = 8.5 was achieved by adding 2 M NaOH solution. The final conductivity of the synthetic HTL-AP (in the order of ca. 10 mS/cm) was similar to the values reported in the literature [11,16,24].

2.2. Membrane filtration setup

A MiniMem filtration setup (PS Prozesstechnik GmbH, Germany) was used for the treatment of synthetic HTL-AP. The flatsheet crossflow membrane module is equipped with a circular NF90 membrane (OD = 6 cm, A = 0.0028 m^2). The volume of the NF module (feed + permeate chambers) is ca. 10 mL. Table 2 lists the general information about the NF90 membrane. Punching of NF90 membranes was performed without surface contact to prevent damage to the thin polyamide active layer (ca. 200 nm [25–27]). Membranes were not removed from the cell until the end of the whole test cycle to avoid any physical damage. Inside the membrane module at the feed side a magnetic stirrer is located with a ~2 mm space from the membrane active layer, which simulates the effect of crossflow shear stress in a large-scale spiral-wound membrane element. Fig. 1a shows the PID of the membrane filtration setup (Fig. 1b and c). Feed is provided to the NF module from TK1 (working volume = 100 mL) using an analytical piston pump. The content of TK1 is homogenized by continuous stirring with the help of a magnetic stirrer and a stirrer bar. During normal operation (or flux measurement), the system is set to concentration (permeate recovery) mode (V01 close, V02 open, solid lines in Fig. 1a–PID), and the permeate is collected in an open vessel (atmospheric), which is weighed using an analytical balance (ML204, Mettler Toledo, Switzerland). Permeate flux was calculated according to Eq. (1) and the permeate recovery percent was calculated using Eq. (2):

$$J = \frac{W_P}{A_m \times t} \quad (1)$$

$$Y = \frac{W_P}{W_F} \times 100 \quad (2)$$

Where J is the permeate flux [L/m^2.hr, assuming water density of 1 g/cm^3], Y is the recovery weight percent [wt%], W_P is permeate weight [g], W_F is Feed weight [g], A_m is membrane area [m^2], and t is filtration time [hr].

During pressure ramp-up and transient-state until reaching steady-state, the system is set to full recirculation mode (V01 open, V02 close, dashed lines in Fig. 1a–PID). In all tests, V03 is regulated manually to create the required TMP in order to operate in a constant TMP (variable flux) mode of operation. During pressure ramp-up, V03 was slowly closed so that the PI2 increase rate would be less than 0.1 bar/s to prevent hydraulic shock to the membrane [25]. At the end of the recovery test, samples were taken from the remaining retentate and the combined permeate for analysis. Rejection performance was calculated according to Eq. (3):

$$R_i = \left(\frac{C_{i,F} - C_{i,P}}{C_{i,F}}\right) \times 100 \quad (3)$$

Where R_i is the rejection percent of the ith component, $C_{i,F}$ is the concentration of the ith component in the feed, and $C_{i,P}$ is the concentration of the ith component in the permeate.

To avoid biased performance comparison due to membrane compaction and irreversible fouling a new membrane was used for each test. All tests were conducted at room temperature. Table 3 provides a summary of the NF system used in this study.

2.3. Membrane fouling analysis

NF90 fouling was analyzed using Darcy's law of permeation and the resistance-in-series model [28] according to Eqs. (4)–(19):

Table 1
Composition and general information of the synthetic HTL-AP.

Compound	MW (Da)	Chemical class	Concentration (mg/L)	Wt%
Acetic acid	60	Carboxylic acid	2000	0.20
Cyclopentanone	86.09	Cyclic Oxygenates	900	0.09
2-Methylpyrazine	94.11	Nitrogenates	850	0.09
3-hydroxypyridine	95.1	Oxygenated aromatics	500	0.05
Levulinic acid	116.01	Carboxylic acid	1100	0.11
Succinic acid	118.09	Dicarboxylic acid	2300	0.23
Oleic acid	282.46	Fatty acids	6800	0.68
Tween 80	1300	Non-ionic surfactant	4 mL in 1 L	0.42
NH_4^+ (mg/L)	18.04	NH_4NO_3 source	4000	0.14
PO_4^{3-} (mg/L)	94.97	$(NH_4)_2HPO_4$ source	1000	1.61

Table 2
General properties of the NF90 nanofiltration used in this study for the treatment of synthetic HTL-AP.

Product	Manufacturer	MWCO	Type	Material	Zeta Potential	Op. pH	Max Op. pressure/ temperature
NF90	DuPont FilmTec™, USA	100–200 Da[1]	TFC	• Active layer: cross-linked polyamide • Support layer: Polysulfone • Backing: non-woven polyester fabric	~ −30 mV (at pH = 7) Isoelectric pH~4.0 [20, 28, 29]	2–11	41 bar, 45 °C

Notes:1–98 % $MgSO_4$ rejection. Test condition: 15 % recovery, 4.8 bar TMP, 2000 ppm $MgSO_4$ solution, 25 °C, pH = 8 [25].

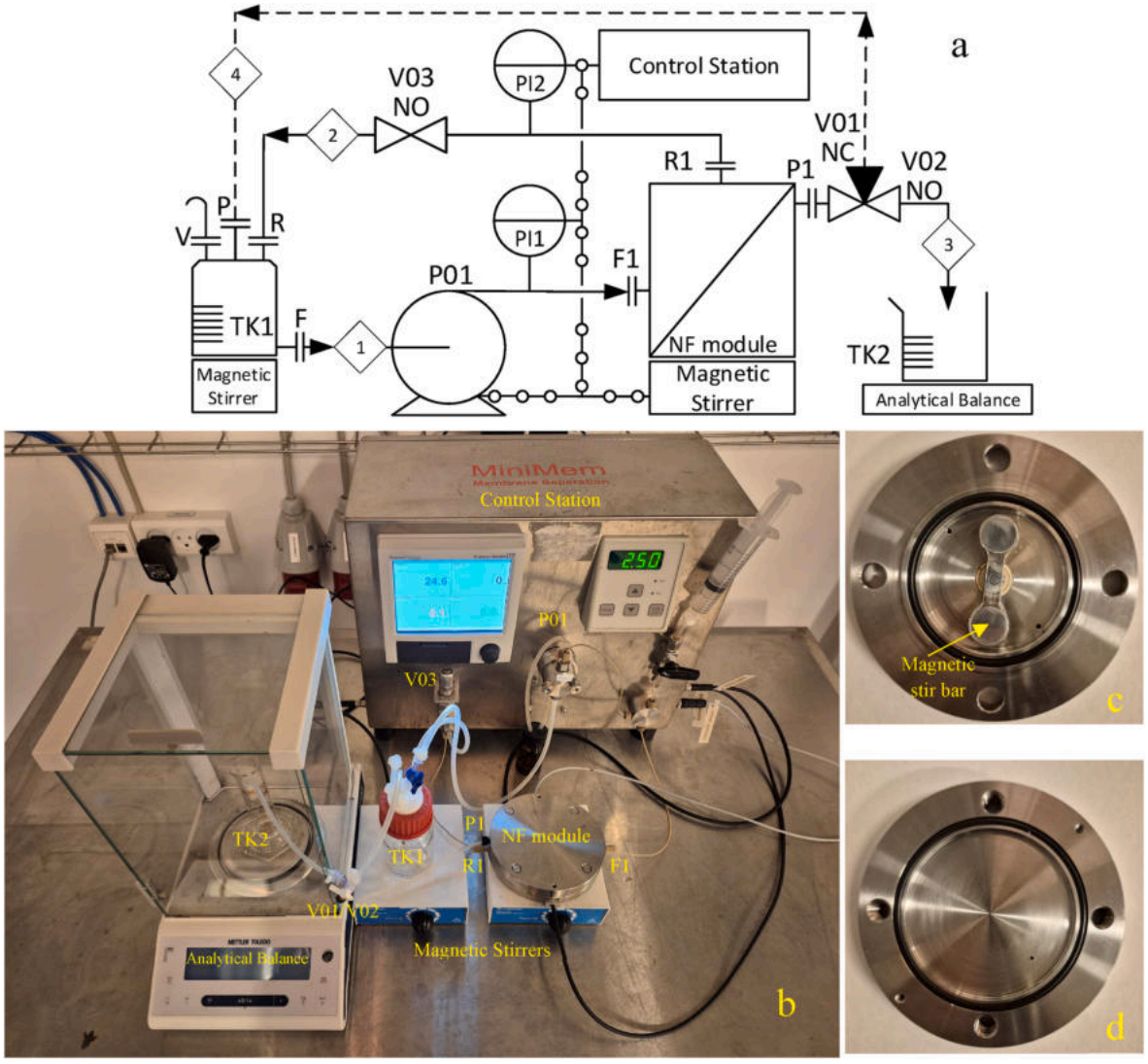

Fig. 1. a) PID representation, b) MiniMem batch membrane filtration unit, c) feed block of NF module, and d) permeate block of NF module. Streams: 1: feed, 2: retentate, 3: permeate (recovery mode), 4: permeate (recirculation mode). Abbreviations: TK1: feed tank, TK2: permeate collection vessel, V: vent nozzle, P: permeate nozzle, R: retentate nozzle, F: feed nozzle, P1: membrane module permeate nozzle, R1: membrane module retentate nozzle, F1: membrane module feed nozzle, V01 (normally closed) and V02 (normally open) permeate position valve, V03: retentate valve (normally open), PI1 and PI2: pressure indicator. P01: feed pump.

$$J = \frac{TMP}{\mu . R} \quad (4)$$

$$R_{Total\_feed} = R_{Membrane} + R_{Concentration\_polarization} + R_{Gel\_layer} + R_{Adsorbed\ foulants/pore\ blockage} + R_{Irreversible} \quad (5)$$

$$R_{Membrane} = \frac{TMP}{\mu . J_0} \quad (6)$$

$$R_{Total\_feed} = \frac{TMP - \Delta\pi}{\mu_{Feed} . J_{Feed}} \quad (7)$$

$$\Delta\pi = \pi_{F/C} - \pi_P \quad (8)$$

$$\pi_{F/C} = \frac{C_{F/C} . (T + 320)}{491000}, C(TDS) < 20000 \frac{mg}{L} \quad (9)$$

Table 3
Summary of operational parameters of the NF system for synthetic HTL-AP treatment.

Parameter	Value (unit)
Operating mode	Crossflow (recovery/ recirculation)
Synthetic HTL-AP recovery, Y	30 wt%
Membrane area and outer diameter	A = 0.0028 m^2 OD = 6 cm
NF module working volume	ca. 10 mL
Feed temperature	25 °C
Feed pressure	26 bars
Feed volume	50 mL
Feed pump flowrate (synthetic HTL-AP and pure water)	2.5 and 10 mL/min
NF module stirrer speed (recovery mode and flushing)	300 and 650 rpm

$$C_{F/C} = C_F \frac{ln\frac{1}{1-\left(\frac{Y}{100}\right)}}{\left(\frac{Y}{100}\right)} \quad (10)$$

$$\pi_P = 1.12(273+T)\sum M_i \rightarrow \pi_P = 1.12(273+T)(M_{Na}+M_{Cl}) \quad (11)$$

$$R_{Total\_water} = \frac{TMP}{\mu_{Water}.J_1} \quad (12)$$

$$R_{Concentration\_polarization} = R_{Total\_feed} - R_{Total\_water} \quad (13)$$

$$R_{Fouling} = R_{Total\_water} - R_{Membrane} \quad (14)$$

$$R_{After\_DI\_flushing} = \frac{TMP}{\mu_{Water}.J_2} \quad (15)$$

$$R_{Gel\_layer} = R_{Total\_water} - R_{After\_DI\_flushing} \quad (16)$$

$$R_{After\_NaOH\_flushing} = \frac{TMP}{\mu_{Water}.J_3} \quad (17)$$

$$R_{Adsorbed\_foulants/pore\_blockage} = R_{After\_DI\_flushing} - R_{After\_NaOH\_flushing} \quad (18)$$

$$R_{Irreversible} = R_{After\_NaOH\_flushing} - R_{Membrane} \quad (19)$$

Where TMP is transmembrane pressure [Pa], Δπ is osmotic pressure difference over the membrane at 30 wt% recovery [Pa] calculated according to DuPont RO/NF manual through Eqs. (8)–(11) [25,29], $\pi_{F/C}$ is osmotic pressure of the feed-concentrate at 30 wt% recovery, T is feed temperature [°C], $C_{F/C}$ is the average total dissolved solids (TDS) concentration of the feed-concentrate at 30 wt% recovery [mg/L], C_F is the average TDS concentration of the feed synthetic HTL-AP [mg/L], M_i is molality [mol/kg] calculated by converting the average permeate TDS to its equivalent NaCl molality, J is the membrane flux [$m^3/m^2.s$], μ_{water} is the viscosity of water ($8.9{\cdot}10^{-4}$) [Pa.s], μ_{Feed} is the viscosity of feed (*vide infra*) [Pa.s], R_i is ith resistance element [1/m]. Since Eq. (9) is valid for saline streams [25,29], Eq. (11) was used for the calculation of permeate osmotic pressure, which is the simplified form of the Van't Hoff equation, generally valid for dilute and ideal aqueous solutions [30–32]. Obtained values for osmotic pressure were cross-checked using Aspen Plus V.14 by using the ELECNRTL property method and by specifying the composition of feed, retentate, and permeate based on the composition of synthetic HTL-AP at both pH levels and rejection values (results not shown here). The DuPont RO/NF manual instructs a maximum 30 wt% permeate recovery per element and 70–75 % recovery for the whole system (normally 2 stages, with 4 pressure vessels. Each pressure vessel contains up to 6 elements) to prevent membranes from extensive fouling [25]. Fig. 2 demonstrates the full experimental work-flow for one cycle of NF treatment of synthetic HTL-AP including consequent pure water flux measurements for fouling behavior analysis. A membrane pre-compaction step was deliberately omitted because compaction naturally occurs during actual operation, and also, according to DuPont, NF90 is a low compaction membrane [33]. Each experiment was repeated 3 times, and the standard deviation (SD) is reported as standard error for flux during concentration mode, rejection performance, and resistance values. Flushing time and cleaning chemicals were selected according to the DuPont RO/NF manual [25]. No backwashing/air-scouring is mentioned in this manual.

The membrane compaction test was performed according to the literature [34,35] by measuring pure water flux at different pressure steps using a neat membrane. Before flux measurements, the system remained in full recirculation mode for 10 min to reach steady state. After each pressure ramp-up and ramp-down cycle the module was filled with water (without disassembling the module and physical contact with the membrane to avoid damage to the membrane active layer) and remained overnight under pressure-release conditions (Zero TMP, no flow) to check if the membrane compaction is reversible. After 3 cycles of compaction tests, $MgSO_4$ rejection of the compacted membrane was compared with rejection performance of the neat membrane based on the datasheet (Table 2).

2.4. Analytical methods

DR3900 spectrophotometer (HACH, USA), LT200 heating block (HACH, USA), and HACH-Lange kits (Germany) were used for COD (LCK314, LCK014), PO_4^{3-} (LCK049, LCK351), and NH_4^+ (LCK305, LCK502) measurement. High range kits were used for analyzing the feed and retentate, while low range kits were used for the permeate in order to reduce the error induced by sample dilution. A portable multimeter (HQ40d, HACH, USA) was used for measurement of pH (using PHC101 electrode), TDS, and conductivity (both using CDC401 electrode). A high-performance liquid chromatography (HPLC) instrument (Dionex Ultimate 3000, Thermo Fisher Scientific, USA) equipped with a refractive index detector (RID) and a PL Aquagel-OH 20 size exclusion chromatography (SEC) column (Agilent, USA) was used to measure the apparent MW distribution of feed and treated synthetic HTL-AP samples [36]. The resolve range of this specific column is from 100 to 20 kDa. The solvent was DI water with an elution rate of 1 mL/min, and the injection volume was 5 μL. The apparent MW distribution was calibrated (R^2 = 0.99) using ReadyCal polyethylene glycol Kits (MW range: 238–44000 Da, Agilent, USA). An attenuated total reflectance-Fourier transform infrared spectroscopy (ATR-FTIR) instrument (Cary 630, Agilent, USA) was used to obtain FTIR spectra of synthetic HTL-AP, neat NF90, and used membranes (before any flushing and using fresh/not dried membrane samples). The spectrum was recorded in the range 650–4000 1/cm at 1 1/cm scan resolution (8 sample scans) in absorbance mode. The neat membrane sample was soaked in DI water for 12 h prior to FTIR analysis. A scanning electron microscope (SEM, Quanta200, FEI/Thermo Fischer, USA) was used for the evaluation of the neat and used NF90 membrane surface morphology at low vacuum mode with Large Field Detector (LFD) detector at 10 kV without metal coating. To prevent damage to the SEM equipment, membrane samples (both neat and used) had to be dried in a desiccator overnight. Simultaneous thermal analysis (STA), which combines thermogravimetric analysis (TGA) with Differential Scanning Calorimetry (DSC), was performed (Alumina Crucible, 25–800 °C, 5 °C/min, N_2 flow: 20 ml/min) on the neat and used membrane samples using the STA 449 F3 Jupiter device (NETZSCH, Germany). A DSA100S instrument (KRUSS, Germany) was used for the measurement of the water/diiodomethane droplet contact angle on the surface of the membrane samples with the sessile drop method. Total surface free energy (surface tension) was calculated using Owens–Wendt two-component surface energy equation [37,38]. A minimum number of 10 droplets (volume of each droplet was 5 and 2 μL for water and diiodomethane, respectively) were tested on

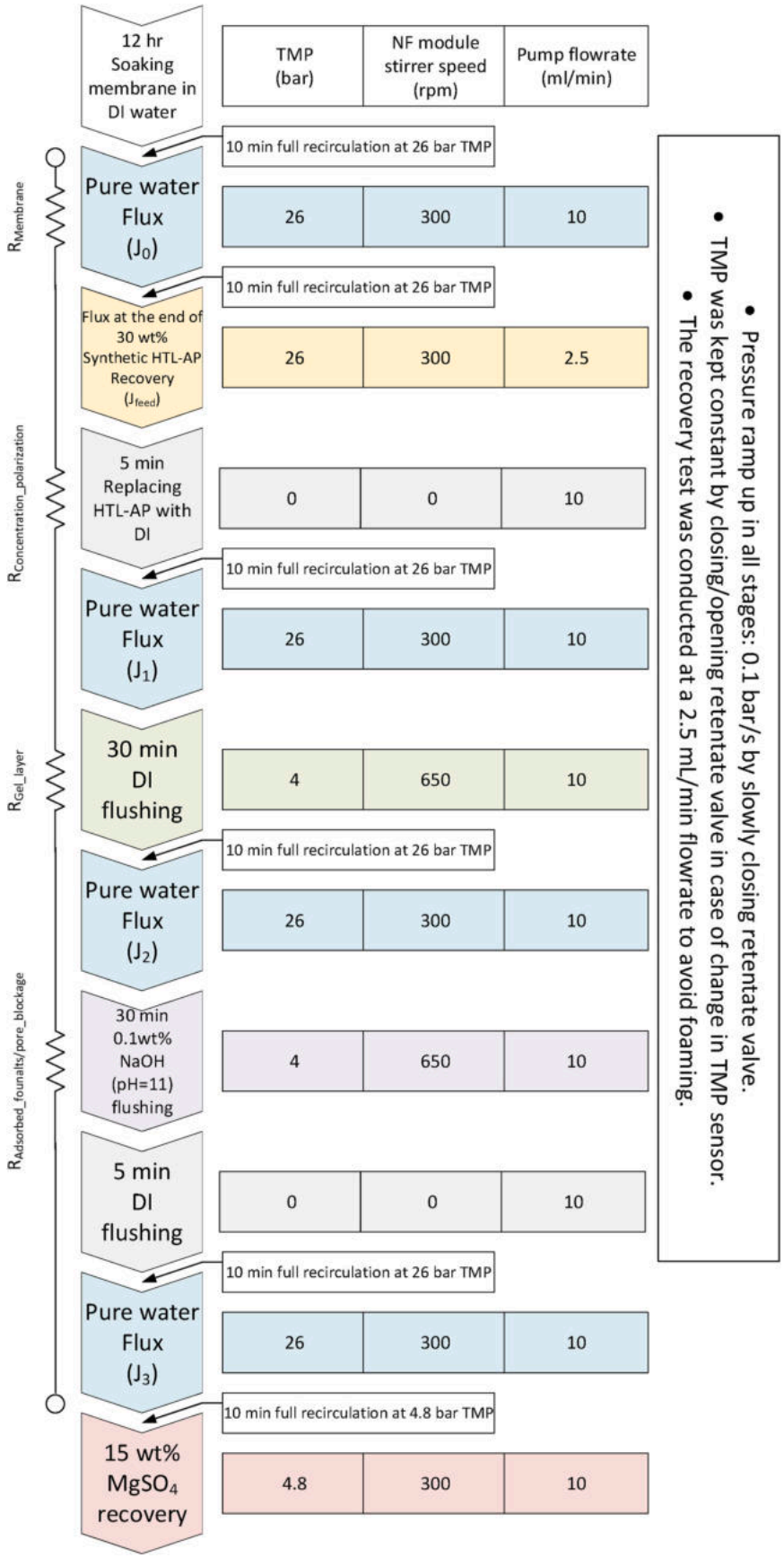

Fig. 2. Experimental protocol for each membrane filtration cycle using the NF90 membrane and synthetic HTL-AP.

each membrane sample, and contact angle calculation was performed 5 times for each droplet. Prior to contact angle and STA measurements, membrane samples were placed in a desiccator overnight to remove any humidity and free water. The neat membrane sample was soaked in DI water for 12 h and then placed in a desiccator overnight. Since membrane samples were very thin, the samples were firmly attached to a microscope glass film using a thin double-sided tape to avoid any bumps, and only the edges of the sample were pressed to the tape to avoid any physical damage to the membrane sample surface. Relative density and viscosity of synthetic HTL-AP at both pH levels were measured at room temperature using a 25 mL pycnometer and a Cannon-Fenske opaque viscometer (size 75, Paragon Scientific, UK), respectively. Moreover, an HR20 Discovery Hybrid Rheometer (TA instrument, USA) equipped with a 20.0 mm 0.994167° cone plate at 25 °C was used to validate results at varying shear rate from 1 to 100 1/s.

3. Results and discussion

3.1. Rejection and synthetic HTL-AP treatment performance

NF90 rejection performance was evaluated in terms of COD, NH_4^+, PO_4^{3-}, conductivity, and TDS (Fig. 3). Detailed mass balance data are gathered in the supplementary information section (Table S1). There was a significant difference in NH_4^+ rejection with a change in the pH level of synthetic HTL-AP. 94 ± 1 % NH_4^+ rejection was achieved for HTL-AP(pH = 4) in comparison to 83 ± 3 % for HTL-AP(pH = 8.5). The main mechanisms behind NH_4^+ rejection are Donnan exclusion, which arises because co-anions such as NO_3^- and PO_4^{3-} are repelled in the synthetic HTL-AP to preserve electroneutrality and maintain coupled ion transport and charge balance, together with steric exclusion resulting from its comparatively large hydrated radius [18,19]. However, according to the $NH_4^+ \leftrightarrow NH_3$ speciation equilibrium, at pH = 8.5, approximately 15 % of NH_4^+ is in the form of NH_3 [26,39]. NH_3 is volatile and can be lost to the headspace during pH adjustment or during filtration. Since LCK305 and LCK502 kits are unable to detect NH_3, the apparent loss of NH_4^+ was accounted for in Table S1 when calculating rejection (ca. 3400 ppm NH_4^+ for HTL-AP(pH = 8.5) vs. 4000 ppm NH_4^+ for HTL-AP(pH = 4)). Based on literature, smaller and charge-neutral NH_3 has more permeability than the NH_4^+ form, which matches the lower NH_4^+ rejection efficiency (ca. 83 %) and higher NH_4^+ concentration (ca. 590 mg/L) in the permeate of NF90 for HTL-AP(pH = 8.5) in comparison to pH = 4 (ca. 94 % and 237 mg/L, respectively) [5,26].

PO_4^{3-} rejection was almost identical (ca. 99 %) at both feed pH values since the rejection of this ion is also dominated by a combination of steric (size) exclusion, as a result of its large hydrated radius [40], and the Donnan effect [18,41]. Also, complexation with organics could be a possible mechanism that reduces the permeability of PO_4^{3-} [41].

There was no significant difference between the COD rejection (ca. 95 %) of NF90 at both pH values, mainly due to the size exclusion of organics and emulsified micelles/droplets, which is confirmed by the SEC results and the apparent MW distributions obtained for feed, permeate, and retentate (Fig. 4, *vide infra*). The remaining organic compounds in the NF permeate are mainly small compounds, e.g., organic acids [12,42].

NF90 had slightly higher TDS/conductivity rejection (as a proxy for total ion concentration) for synthetic HTL-AP(pH = 4). This observation is due to: 1) higher ionic strength and weakened Donnan exclusion because of membrane charge shielding [19,43], further, since NaOH was used to adjust the pH level of the synthetic HTL-AP from 4 (as-is solution pH) to 8.5, higher TDS/conductivity due to the presence of Na^+ ions was observed for synthetic HTL-AP(pH = 8.5) (Table S1); for synthetic HTL-AP at pH = 8.5, 2) higher permeability of neutral NH_3 at pH = 8.5 (*vide supra*), 3) to some extent, fouling and therefore improved salt rejection (*vide infra*) [44]. But overall, the difference was not significant, and >ca. 85 % TDS/conductivity rejection was achieved.

Apparent MW distribution (Fig. 4) shows a broad distribution for synthetic HTL-AP. In a similar study, Zhang et al. [14] analyzed real HTL-AP samples (produced from HTL using multiple feedstocks such as swine manure and algae) using SEC and obtained a wide distribution ranging from just under 100 to slightly over 10,000 Da. In addition, Fig. 4 shows a clear reduction of permeate peaks in comparison to feed and retentate for synthetic HTL-AP at both pH levels, which confirms earlier rejection results (Fig. 3 and Table S1). The peak at 100–1000 Da in the permeate curves might be attributed to the formation of micelles in the permeate by the organic molecules that were able to pass NF90 (permeate COD is ca. 1500 mg/L, refer to Table S1). The peak at around 10 Da is related to all soluble salts and ions that come out of the column as a single broad peak (MW distribution of synthetic HTL-AP using only salts, without organics, is also included for better comparison). The reason why the intensity of retentate peaks is not larger than the feed might be due to the fact that part of the pollutants remains attached to the surface (in the form of adsorbed foulants, pore blockage, and surface gel fouling layer). Kizza and Eskicioglu [13] studied the fractionation of HTL-AP derived from municipal sludge using UF to analyze its MW

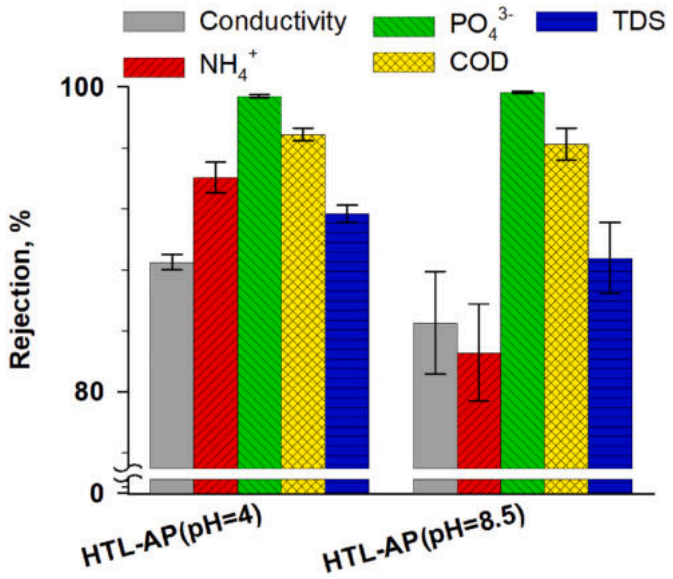

Fig. 3. Rejection performance of the NF90 membrane while treating synthetic HTL-AP. The error bars represent the SD (n = 3).

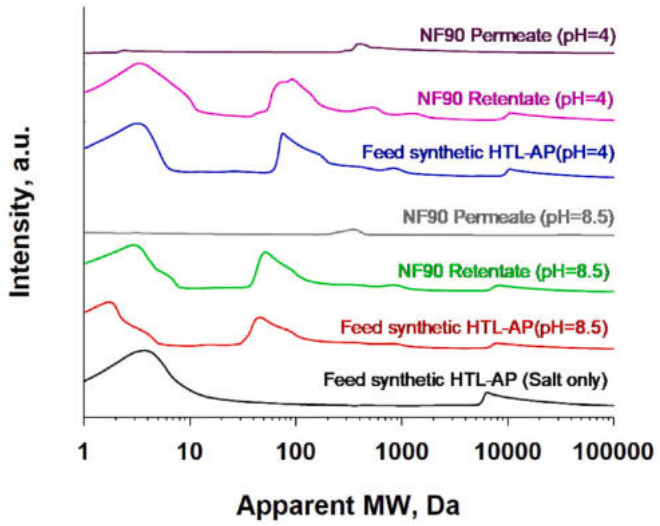

Fig. 4. Apparent molecular weight distribution of synthetic HTL-AP, NF90 retentate, and permeate.

distribution and anaerobic biodegradability. The HTL-AP was processed through UF PES membranes with MWCOs of 300, 100, 10, and 1 kDa in a cascading series. The results revealed that almost 90 % of HTL-AP constituents (such as volatile fatty acids, short-chain fatty acids, soluble COD, phenolic compounds, etc.) can be recovered/concentrated, and the rest is lost due to adsorption to the membrane surface and gel layer fouling. Likewise, in the current study, it was not possible to close the mass balance since, in batch-recycling mode, the amount of material retained in the gel or fouling layer is also uncertain, and quantifying it was out of the scope of the current study.

Overall, approximately 90 % pollutant rejection is achieved with slightly improved rejection performance at pH = 4. The overall permeate quality, for example the permeate COD level (ca. 1500 mg/L), is similar to untreated urban wastewater [5,45] used as a cultivation medium and nutrient source for algae biomass intended as feedstock for HTL [1,5,22]. Accordingly, there could be significant potential to close the water loop in the HTL process by avoiding HTL-AP dilution and reuse NF-treated HTL-AP directly.

3.2. Flux behavior analysis

The permeate flux (Fig. 5) during HTL-AP recovery showed a significant difference with variation of the feed pH level, with pH = 8.5 showing a smaller $J/J_{initial}$ drop (ca. 22 %) than pH = 4 (ca. 43 %). This flux drop is associated with increased osmotic pressure at higher recovery values (i.e., more concentrated feed) and fouling. Because NF90 has a moderately hydrophobic polyamide active layer [20,46], hydrophobic organics (e.g., oleic acid), i.e., solutes with a high Octanol-water partition coefficient ($LogK_{ow}$), exhibit strong hydrophobic interactions with the membrane, leading to adsorption and fouling. However, compounds with low or negative $LogK_{ow}$ are strongly hydrophilic and show lower interaction. Moreover, at pH > 4, the NF90 surface is negatively charged due to the deprotonation of carboxyl and amide groups [20,26], and at pH = 8.5, the intensity of negative charges is larger than at pH = 4 [12,47]. Moreover, weak organic acids and many other organic substances will be mostly deprotonated (negatively charged) at pH = 8.5 ($\gg pK_a$) [12,25]. Therefore, electrostatic repulsion (Donnan exclusion) could reduce the adsorption/attachment of deprotonated organics on the NF90 membrane surface [14,20,48] at higher pH. Neutral organics (ketones, oleic acid, and tween-80) though can still interact with the membrane surface via hydrophobic interactions. On the other hand, organic compounds in synthetic HTL-AP are mostly neutral/unionized

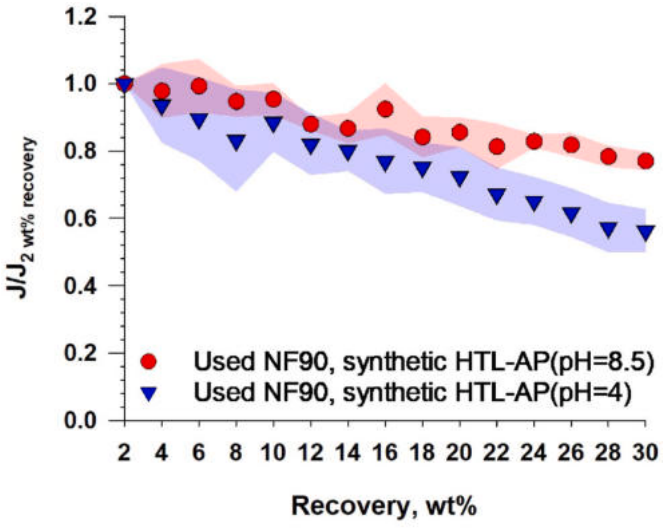

Fig. 5. Normalized permeate flux evolution during 30 wt% recovery of synthetic HTL-AP using NF90. For operational parameters, refer to Fig. 2. The shaded area represents the SD (n = 3).

at pH = 4 (pH < pK_a) [20,42]. Moreover, at pH = 4, the NF90 surface is at/near the neutral point [47,49]. Therefore, at pH = 4, hydrophobic interaction, hydrogen bonding, and van der Waals forces could lead to the adsorption/attachment of organic compounds on the surface of NF90 membrane, which results in more fouling [46,50]. This could be assisted further due to the presence of hydrophobic neutrals (such as ketones) and non-ionic surfactants, and in the case of the current study, Tween-80 as a non-ionic surfactant. Table S2 provides a summary of the NF90 membrane charge, solute ionization status, pK_a, $LogK_{ow}$, and earlier discussed interactions at the studied pH levels. In addition, relative viscosity and density values were 1.1 ± 0.1 cP/995 ± 8 kg/m^3 and 1.23 ± 0.07 cP/1004 ± 5 kg/m^3 for synthetic HTL-AP(pH = 4) and pH = 8.5, respectively. The differences were not statistically significant (p-value>0.05, n = 5), and the synthetic HTL-AP exhibited water-like behavior over the investigated shear-rate range. This behavior is attributed to the low concentration of organic pollutants (<2 wt%) and confirming a dilute, well-dispersed emulsion. Consequently, the improved fouling performance of NF90 using synthetic HTL-AP(pH = 8.5) cannot be attributed to changes in bulk viscosity/density as a result of pH change.

To elucidate the mechanism of the observed fouling, a systematic comparison of pure water flux was conducted according to the experimental protocol presented in Fig. 2. Total membrane fouling was higher in the case of synthetic HTL-AP(pH = 4) compared to pH = 8.5 ($9.8{\cdot}10^{14}{\pm}8{\cdot}10^{13}$ vs. $5.5{\cdot}10^{14}{\pm}5{\cdot}10^{13}$ 1/m, respectively). The difference in fouling resistance (Fig. 6) showed that at both pH levels, reversible fouling, including concentration polarization, gel layer, and foulants adsorption/pore blockage, is the major players causing flux decline, and NaOH flushing will almost restore the original pure water flux by increasing the negative charge of NF90 through deprotonation of carboxyl groups in polyamide layer, which enhances electrostatic repulsion between foulants and the membrane surface, and through foulant hydrolysis/dissolution [17,51]. Irreversible fouling, probably due to membrane compaction, highly persistent adsorbed foulants, and irreversible pore blockage, led to insignificant membrane fouling. However, at pH = 4, the share of the gel layer resistance of the total fouling resistance is higher than synthetic HTL-AP(pH = 8.5) (ca. 32 vs. 14 %, respectively), which matches the lower flux of NF90 using HTL-AP (pH = 4) (Fig. 5). On the other hand, concentration polarization has a higher share at pH = 8.5 compared to synthetic HTL-AP(pH = 4) (ca. 24 vs. 13 %, respectively), which matches the slightly lower rejection performance of NF90 using HTL-AP(pH = 8.5) (Fig. 3). Moreover, all of the used membranes showed ca. ~98 % $MgSO_4$ rejection after the NaOH flushing step, which was similar to the rejection performance of the neat membrane. Compaction tests (Fig. 7) revealed that at higher TMP values, the membrane suffers some degree of compaction. Compacted NF90 membrane after 3 compaction cycles showed ca. ~98 % $MgSO_4$ rejection, which was similar to the rejection performance of the neat membrane.

3.3. Membrane autopsy

The results of the resistance-in-series model analysis (Fig. 6) suggest the presence of a thin fouling gel layer on the surface of the NF90 membrane after synthetic HTL-AP treatment. Since the contribution from pore blockage/persistent adsorbed foulants remained unchanged at both pH levels, and commonly used pore size distribution techniques, such as N_2 adsorption–desorption (using BET/BJH models), may not be applicable to TFC membranes with a dense polymeric active layer, the pore size distribution of the used membranes was not investigated further [51,52]. Since no visible fouling layer was observed on the surface of used NF90 membranes (Fig. S2), to confirm gel layer presence, the change in the surface chemistry and functional groups of the used membranes was compared to neat NF90 membranes using ATR-FTIR, which is sensitive to surface changes due to its shallow sample penetration [53] (Fig. 8). In addition, the spectrum of synthetic HTL-AP

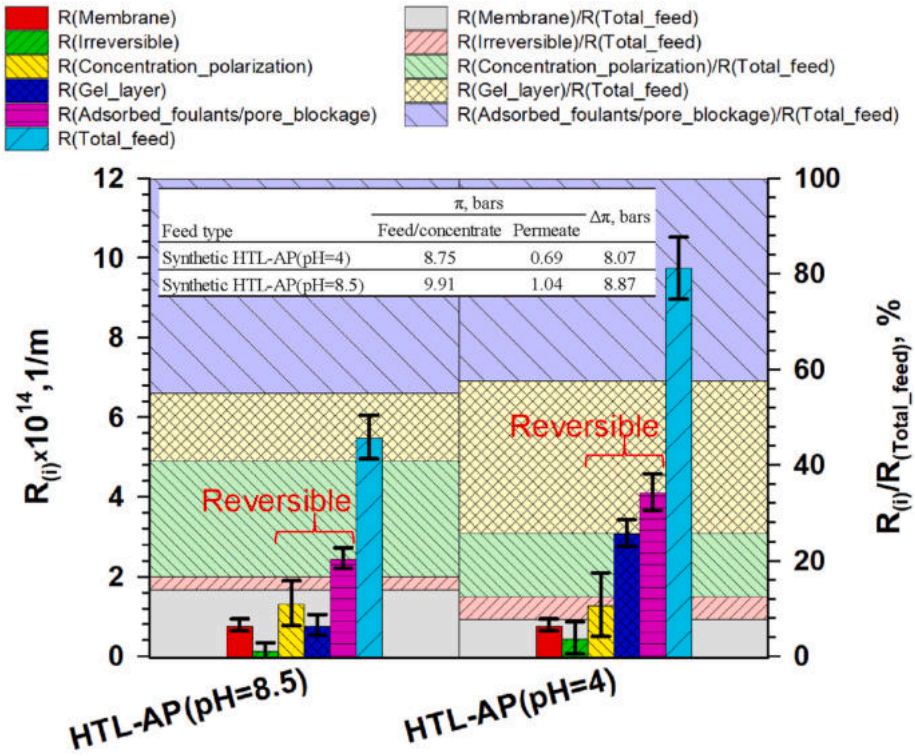

Fig. 6. Fouling analysis and distribution of resistance values of used NF90 membranes according to the resistance-in-series model. The error bars represent the SD (n = 3). The table in the inset shows the calculated osmotic pressures using Eqs. (8)–(11).

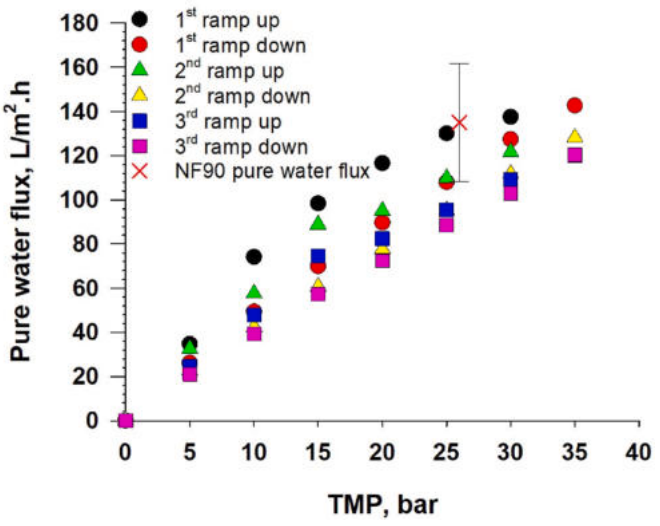

Fig. 7. NF90 membrane compaction results using pure water. Operational parameter: module rpm = 300, T = 25 °C, pump flowrate = 10 mL/min. The error bars represent the SD (n = 3).

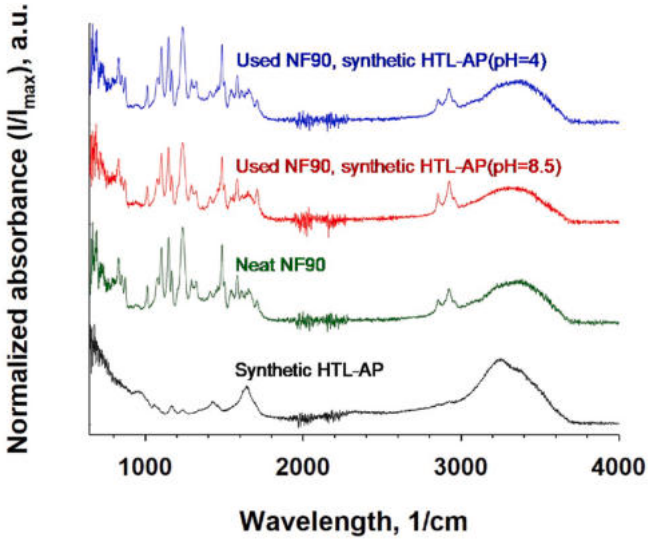

Fig. 8. FTIR spectra of synthetic HTL-AP, neat NF90 membrane, and used (before any flushing) NF90 membranes.

(as-is, pH = 4) was obtained. The following functional groups can be detected for the neat NF90 membranes: 1) carbonyl (C═O, amide I) groups at 1650, 2) C–O stretching at 1016, 3) aromatic double-bonded carbon (C═C) at 1492, 4) asymmetric and symmetric O═S═O (sulfone group) stretch at 1150, 1320, 5) N–H stretching (in –CO–NH- groups) overlapped with O–H (adsorbed water and hydroxyl containing foulants) at 3200–3500, 6) C–N stretch (amide III) at 1220–1300, 7) aromatic C–H bending at 700–900, 8) N–H bend and C–N stretch (amide II) at 1550, and 9) aliphatic bands (-CH_2 and –CH) at 2800–2900 1/cm [18,53–56]. ATR-FTIR spectra of the used NF90 membranes (before DI flushing, without drying) showed no new peaks, and an insignificant change in the intensity of peaks in the spectrum of the neat membrane was detected (probably due to very similar peaks of the synthetic HTL-AP and NF90 membrane). The presence of sulfone groups (from the microporous support layer) in the spectrum of the used membranes confirms the thin nature of the fouling layer [53,57,58]. Since both the fouling layer and the NF90 polyamide active layer are extremely thin, the IR light was able to pass through them and reach the polysulfone microporous support layer beneath [26]. Accordingly, based on the results of the resistance in series model, the assumption that only a thin fouling gel layer forms during treatment of synthetic HTL-AP is

confirmed (Fig. 6).

To visually confirm the presence of a thin fouling gel layer, the surface morphology of used NF90 membranes was compared to a neat membrane using SEM. Fig. 9a shows the characteristic ridge and valley morphology of the neat NF90 membrane [53,56,59]. In the present study the used membranes were first dried in a desiccator, which leads to physical disruption of the actual gel layer after the fouling test. Due to limitations of the SEM instrument and the risk of damage caused by high water content under vacuum, it was not possible to analyze the membrane samples before drying and environmental SEM (ESEM) did not provide high-quality images (results not shown here), as they were blurred and low in resolution. However, Fig. 9b and c (SEM of used NF90 for treatment of synthetic HTL-AP at pH = 4 and 8.5, respectively) reveal a smoother surface covered by a continuous and homogeneous fouling layer without evidence of discrete particles. This suggests fouling is not governed by conventional particulate cake formation. Given the

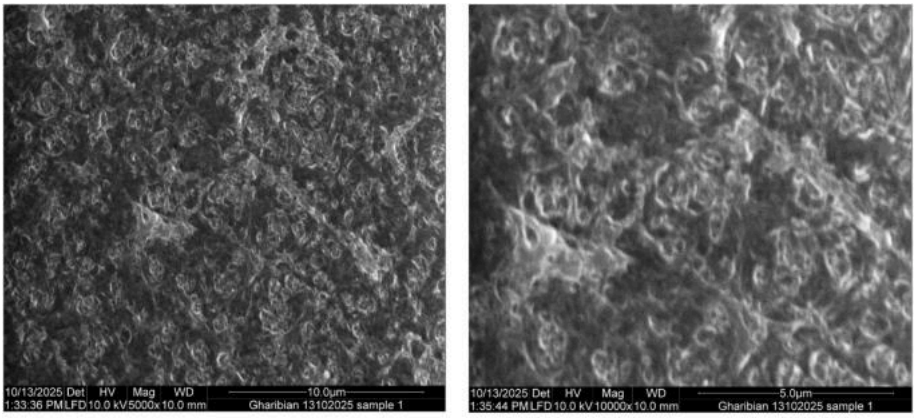

a) Neat NF90 membrane

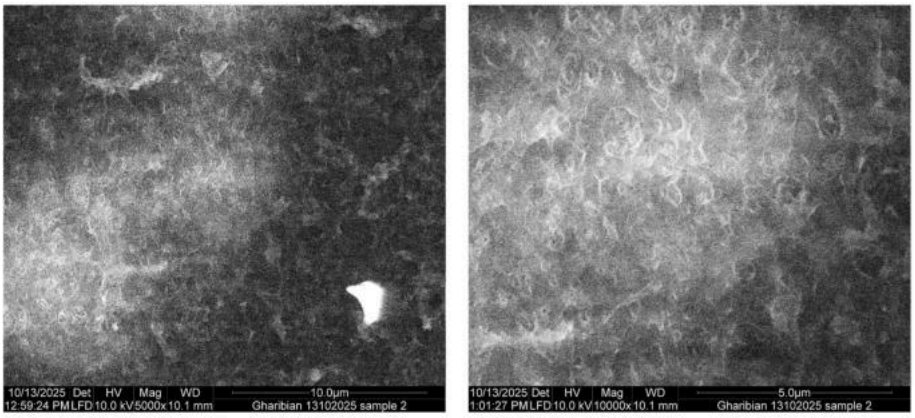

b) Used NF90, synthetic HTL-AP(pH=4)

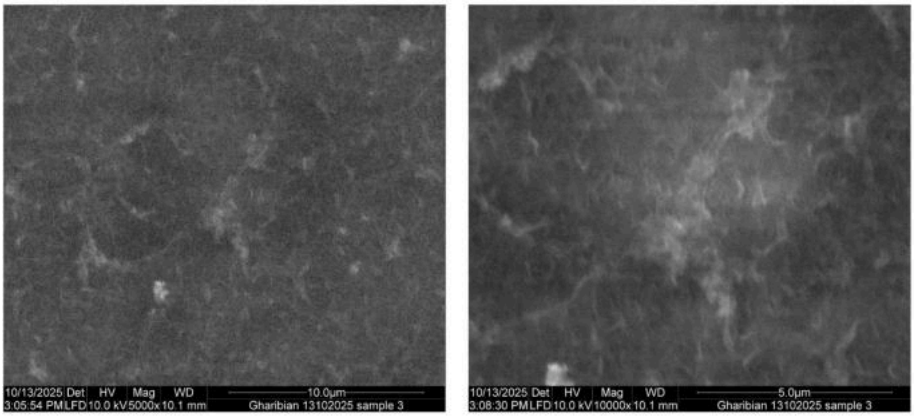

c) Used NF90, synthetic HTL-AP(pH=8.5)

Fig. 9. SEM microimages (5 kx and 10 kx magnification) of the neat and used NF90 membranes after synthetic HTL-AP treatment.

predominance of micellar and dissolved organic constituents and lack of suspended particles in the synthetic HTL-AP, the morphology is consistent with gel-like fouling behavior rather than rigid cake deposition. This is in line with several studies that have attributed the observed smoother surface on NF90 membranes after organic fouling to gel layer formation [47,56,60].

Contact angle measurements (Fig. 10) revealed a value of 80 ± 3° (<90°) for the neat NF90 membrane, indicating weak hydrophilicity, which is consistent with the values reported in the literature [20,46,54]. Water contact angle of the used membrane sample used for synthetic HTL-AP treatment was 62 ± 4° and 63 ± 4° for pH = 4 and 8.5, respectively. The significant difference between the contact angles of the neat and used membranes shows a change in the surface properties of the used membranes after synthetic HTL-AP treatment, probably due to the presence/adsorption of hydrophilic organic foulants in the polymer matrix [50,54,57], specifically Tween-80 in the form of a thin gel layer on the membrane surface, which was previously confirmed by FTIR (Fig. 8) and SEM (Fig. 9) analyses. The difference between the contact angle of the used membrane sample for treatment of synthetic HTL-AP at pH = 4 and 8.5 was not significant, probably due to the thin nature of the gel layers and similar feed composition. Comparing the contact angle of water and diiodomethane revealed that the total surface free energy (surface tension) value increased from 35 to 48 and 49 mN/m for the neat membrane, the used NF90 membrane for synthetic HTL-AP at pH = 4, and at pH = 8.5, respectively (for polar and dispersive components refer to Table S4). The increase in the surface energy shows that the membrane is more chemically active, and this increase is mainly due to the increase in the polar component. This confirms that the used membranes have more polar or hydrophilic functional groups on their surfaces, which supports the presence of a thin gel layer [53,61].

TGA profiles (Fig. 11a) of the neat and used membranes show the first degradation step until 100 °C, related to adsorbed moisture loss, which is negligible considering that all samples were dried in a desiccator. The second stage occurs between 100 to ca. 400 °C, which is attributed to the decomposition of foulants (gel layer, adsorbed foulants, and pore blockage) and is more profound for the used NF90 for synthetic HTL-AP(pH = 4). The two fast (Fig. 11b) decomposition steps after 400 and up to 550 °C are attributed to the decomposition of polyamide (≈400 °C) and polysulfone (≈500 °C) polymers [54,62]. The heat-flow response (Fig. 11c), including both endothermic and exothermic events, differed between the neat and fouled membranes, indicating that fouling

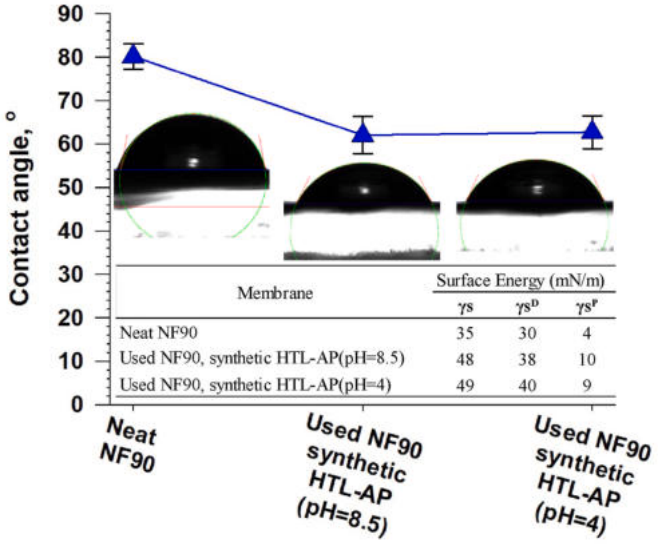

Membrane	Surface Energy (mN/m)		
	γs	γs^D	γs^P
Neat NF90	35	30	4
Used NF90, synthetic HTL-AP(pH=8.5)	48	38	10
Used NF90, synthetic HTL-AP(pH=4)	49	40	9

Fig. 10. Results of water droplet contact angle on neat and used NF90 membranes. The error bars represent the SD (n = 10). The inset images represent only a sample of the 10 measurements performed.

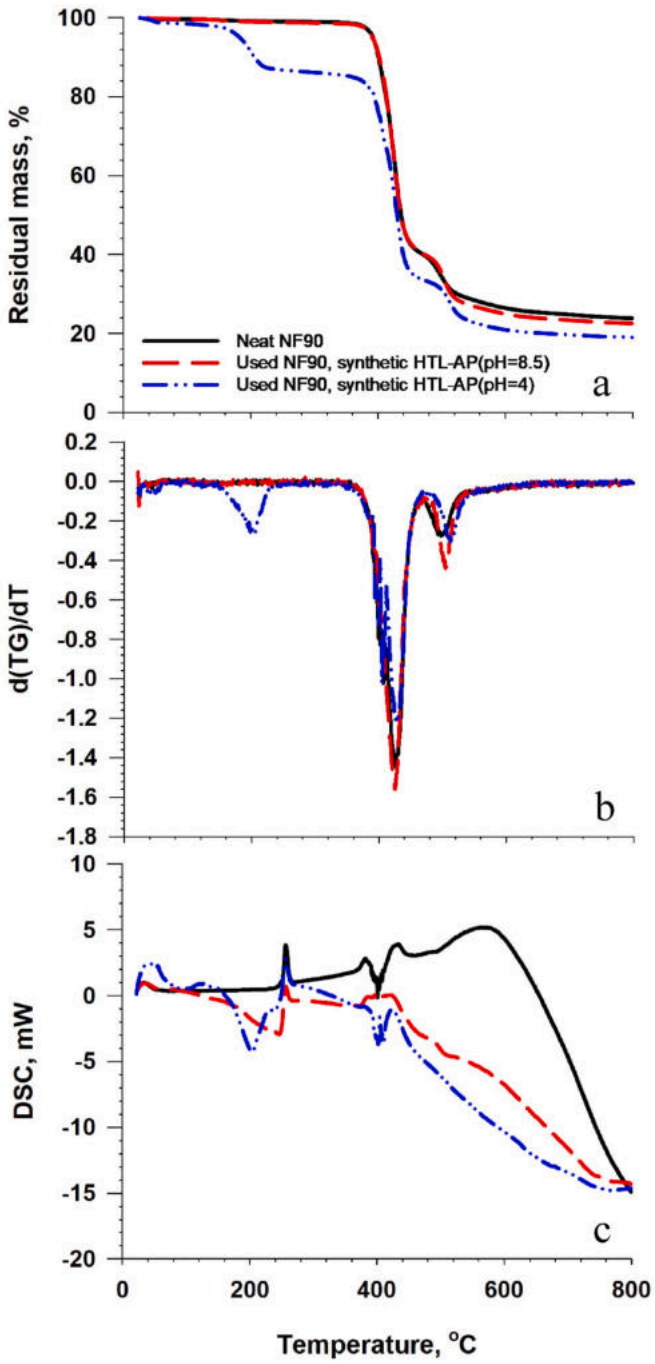

Fig. 11. Results of STA analysis on the neat and used NF90 membranes, a) TGA, b) DTG, and C) DSC.

altered the thermal behavior. The used NF90 for synthetic HTL-AP(pH = 8.5) exhibits only a minor deviation from the TGA profile of the neat membrane, which includes a slight broadening of the polyamide DSC/DTG peak, a very small early mass-loss shoulder, and slightly lower residual mass than the neat NF90 sample, indicating that only a negligible amount of foulant is present. In contrast, the used NF90 for synthetic HTL-AP(pH = 4) shows pronounced changes across all analyses, including a clear low-temperature endothermic/DTG feature (≈200–250 °C), significantly larger mass loss prior to polymer degradation, and a lower final residual mass, demonstrating the presence of volatile and thermally active organic deposits which require heat input (endothermic).

4. Conclusion

In this study, the treatment of synthetic HTL-AP using a DuPont NF90 polyamide NF membrane was evaluated with particular emphasis on membrane rejection and fouling behaviour analysis supported by membrane autopsy. Almost complete PO_4^{3-} and COD removal were achieved. NH_4^+ rejection performance was better for synthetic HTL-AP (pH = 4) (94 ± 1 %) than pH = 8.5 (83 ± 3 %) due to the presence of a gel layer and the conversion of some NH_4^+ to NH_3 (with better permeability). More than 85 % TDS/conductivity rejection was also achieved. The quality of the obtained permeate was similar to that of untreated urban wastewater used as a cultivation medium for algae biomass intended as feedstock for HTL. The apparent MW distribution from SEC confirmed the above-mentioned NF90 rejection performance. Flux monitoring and the resistance-in-series model revealed that irreversible fouling (due to membrane compaction, persistent adsorbed foulants, and pore blockage) was negligible. Reversible concentration polarization and gel layer fouling were the major contributors to NF90 fouling. Persistent foulants that were not removed by water flushing were efficiently removed by 0.01 wt% NaOH flushing. The contribution of the gel layer to the total fouling was larger for synthetic HTL-AP(pH = 4) than at pH = 8.5 due to the hydrophobic interaction of unionized organic compounds with the almost neutral NF90 at pH = 4. FTIR, SEM, TGA, and contact angle autopsy tests collectively confirmed the presence of a thin fouling gel layer on NF90. Since the synthetic HTL-AP model wastewater can be classified as oily wastewater, the results are broadly relevant to oily wastewater treatment involving water-soluble organics, low amounts of emulsified oils, oil micelles, and coexisting organic and inorganic pollutants, including real HTL-AP generated during biocrude production. As these results are promising, future studies should be performed including the following: 1) Optimization of operational parameters in the allowable operating range (design pressure, temperature, and pH) for maximum rejection and lowest membrane fouling, 2) Extension of the number of synthetic HTL-AP fouling/cleaning cycles after NaOH washing (i.e., 5 cycles) to observe the long-term performance of the NF90 membrane, 3) Monitoring single-component rejection using liquid chromatography-mass spectroscopy (LC-MS), 4) evaluating pore size distribution of the used membranes as evidence of pore blockage, 5) Extension to a real HTL-AP with a more complex matrix and NF permeate toxicity assessment for feed biomass HTL algae cultivation, 6) recirculation of NF reject stream back to HTL reactor or further valorization, 7) Scale-up using the spiral-wound elements to reach higher recovery (70–75 %) using multistage systems (with multiple pressure vessels at each stage).

CRediT authorship contribution statement

Soorena Gharibian: Writing – review & editing, Writing – original draft, Visualization, Methodology, Investigation, Formal analysis, Data curation, Conceptualization. **Knud Villy Christensen:** Writing – review & editing, Validation, Supervision, Resources, Project administration, Methodology, Funding acquisition, Conceptualization. **Rime Bahij:** Writing – review & editing, Validation, Supervision, Resources, Methodology, Conceptualization. **Morten Enggrob Simonsen:** Writing – review & editing, Software, Resources, Formal analysis, Data curation. **Massimiliano Errico:** Writing – review & editing, Validation, Supervision, Resources, Project administration, Methodology, Funding acquisition, Conceptualization.

Declaration of competing interest

The authors declare the following financial interests/personal relationships which may be considered as potential competing interests: Massimiliano Errico reports financial support was provided by European Commission. If there are other authors, they declare that they have no known competing financial interests or personal relationships that could have appeared to influence the work reported in this paper.

Acknowledgments

The authors would like to extend their gratitude to Per Morgen for conducting SEM/ESEM imaging. This project has received funding from Horizon Europe, the European Union's Framework 627 Programme for Research and Innovation, under Grant Agreement No. 101122363 (SUSTEPS). Views and opinions expressed are, however, those of the authors only and do not necessarily reflect those of the European Union or the granting authority, CINEA. Neither the European Union nor CINEA can be held responsible for them.

Appendix A. Supplementary data

Supplementary data to this article can be found online at https://doi.org/10.1016/j.memsci.2026.125178.

Data availability

Data will be made available on request.

References

[1] J. Watson, et al., Valorization of hydrothermal liquefaction aqueous phase: pathways towards commercial viability, Prog. Energy Combust. Sci. 77 (2020) 100819.
[2] T. Nguyen, et al., Valorization of the aqueous phase from hydrothermal carbonization of different feedstocks: challenges and perspectives, Chem. Eng. J. 472 (2023) 144802.
[3] M. Usman, et al., From biomass to biocrude: innovations in hydrothermal liquefaction and upgrading, Energy Convers. Manag. 302 (2024) 118093.
[4] W. Farooq, Sustainable production of microalgae biomass for biofuel and chemicals through recycling of water and nutrient within the biorefinery context: a review, GCB Bioenergy 13 (6) (2021) 914–940.
[5] T. Costa, et al., Valorizing hydrothermal liquefaction aqueous phase via nanofiltration: enhancing biocrude production from algal biomass, Bioresour. Technol. (2025) 132456.
[6] A. Agarwalla, K. Mohanty, A critical review on the application of membrane technology in microalgal harvesting and extraction of value-added products, Sep. Purif. Technol. (2024) 127180.
[7] Y. Jiang, et al., Aqueous-phase product treatment and monetization options of wet waste hydrothermal liquefaction: comprehensive techno-economic and life-cycle GHG emission assessment unveiling research opportunities, Bioresour. Technol. 397 (2024) 130504.
[8] L. Leng, et al., Bioenergy recovery from wastewater produced by hydrothermal processing biomass: progress, challenges, and opportunities, Sci. Total Environ. 748 (2020) 142383.
[9] A. Swetha, et al., Review on hydrothermal liquefaction aqueous phase as a valuable resource for biofuels, bio-hydrogen and valuable bio-chemicals recovery, Chemosphere 283 (2021) 131248.
[10] Y. Gu, et al., Advances in energy systems for valorization of aqueous byproducts generated from hydrothermal processing of biomass and systems thinking, Green Chem. 21 (10) (2019) 2518–2543.
[11] A. Sayegh, et al., Treatment of hydrothermal liquefaction wastewater with ultrafiltration and air stripping for oil and particle removal and ammonia recovery, J. Water Process Eng. 44 (2021) 102427.
[12] X. Zhang, et al., Advanced treatment of hydrothermal liquefaction wastewater with nanofiltration to recover carboxylic acids, Environ. Sci.:Water Res. Technol. 4 (4) (2018) 520–528.
[13] R. Kizza, C. Eskicioglu, Ultrafiltration fractionation of potentially inhibitory substances of hydrothermal liquefaction aqueous phase derived from municipal sludge, Water Res. 257 (2024) 121703.
[14] X. Zhang, et al., Fouling mitigation and carbon recovery in nanofiltration processing of hydrothermal liquefaction aqueous waste stream, J. Membr. Sci. 614 (2020) 118558.
[15] S. Gharibian, M. Errico, K.V. Christensen, Towards sustainable bio-oil production: recycling and separation techniques applied to the aqueous phase byproduct of algae biomass hydrothermal liquefaction, Sep. Purif. Technol. (2025) 134493.
[16] K. Szkadłubowicz, et al., Removal of contaminants from liquid after the hydrothermal carbonization of sewage sludge using a combination of membrane techniques and struvite precipitation, Water Resour. Ind. 33 (2025) 100285.
[17] A. Sayegh, et al., Treatment of hydrothermal-liquefaction wastewater with crossflow UF for oil and particle removal, Membranes 12 (3) (2022) 255.
[18] Z. Anari, et al., Pressure-driven membrane nutrient preconcentration for downstream electrochemical struvite recovery, Sep. Purif. Technol. 309 (2023) 122907.
[19] A. Popova, et al., Evaluating the potential of nanofiltration membranes for removing ammonium, nitrate, and nitrite in drinking water sources, Water Res. 244 (2023) 120484.

[20] S. Jamil, et al., Comparing nanofiltration membranes effectiveness for inorganic and organic compounds removal from a wastewater-reclamation plant's micro-filtered water, Mater. Today Proc. 47 (2021) 1389–1393.
[21] R.B. Madsen, et al., Predicting the chemical composition of aqueous phase from hydrothermal liquefaction of model compounds and biomasses, Energy Fuels 30 (12) (2016) 10470–10483.
[22] L. Leng, et al., Use of microalgae to recycle nutrients in aqueous phase derived from hydrothermal liquefaction process, Bioresour. Technol. 256 (2018) 529–542.
[23] Y. Kulikova, et al., Aqueous phase from hydrothermal liquefaction: composition and toxicity assessment, Water 15 (9) (2023) 1681.
[24] A. Sayegh, et al., Membrane distillation as a second stage treatment of hydrothermal liquefaction wastewater after ultrafiltration, Sep. Purif. Technol. 285 (2022) 120379.
[25] DuPont, Filmtec™ Reverse Osmosis Membranes Technical Manual, Form No. 45-D01504-en, Version 18, 2025.
[26] S. Shahgodari, J. Llorens, J. Labanda, Study of total ammoniacal nitrogen recovery using polymeric thin-film composite membranes for continuous operation of a hybrid membrane system, Polymers 17 (12) (2025) 1696.
[27] H.-J. Kim, et al., Application of desalination membranes to nuclide (Cs, Sr, and Co) separation, ACS Omega 5 (32) (2020) 20261–20269.
[28] J. Park, et al., Evaluation of fouling in nanofiltration for desalination using a resistance-in-series model and optical coherence tomography, Sci. Total Environ. 642 (2018) 349–355.
[29] S.G. Salinas-Rodríguez, J.C. Schippers, M.D. Kennedy, Basic principles of reverse osmosis, Seawater Reverse Osmosis Desalination: Assessment and Pre-treatment of Fouling and Scaling 2021 (2021) 59–83.
[30] M.W. Haefner, M.N. Haji, Integrated pumped Hydro reverse osmosis System optimization with enhanced reverse osmosis modeling, in: Volume 23: Sustainable Energy Solutions for a post-COVID Recovery Towards a Better Future: Part VI, 2021. Energy Proceedings.
[31] E. Nagy, et al., The need for accurate osmotic pressure and mass transfer resistances in modeling osmotically driven membrane processes, Membranes 11 (2) (2021) 128.
[32] M. Khraisheh, et al., Osmotic pressure estimation using the Pitzer equation for forward osmosis modelling, Environ. Technol. 102 (16) (2020) 4412–4439.
[33] DuPont, Filmtec™ NF90-4040 Product Data Sheet, 2025.
[34] I.K. Koo, M.N. Chong, K. Goh, Gradient or no gradient: spatial hydrostatic pressure distributions in bilayer thin-film composite membranes, J. Membr. Sci. 727 (2025) 124023.
[35] J. Wu, et al., Role of transmembrane pressure and water flux in reverse osmosis composite membrane compaction and performance, Environ. Sci. Technol. 59 (17) (2025) 8856–8866.
[36] A. De la Rubia, et al., Removal of natural organic matter and THM formation potential by ultra-and nanofiltration of surface water, Water Res. 42 (3) (2008) 714–722.
[37] C. Rulison, Two-component surface energy characterization as a predictor of wettability and dispersability, KRUSS Application note AN213 (2000) 1–22.
[38] D.K. Owens, R. Wendt, Estimation of the surface free energy of polymers, J. Appl. Polym. Sci. 13 (8) (1969) 1741–1747.
[39] K. Emerson, et al., Aqueous ammonia equilibrium calculations: effect of pH and temperature, J. Fish. Res. Board Can. 32 (12) (1975) 2379–2383.
[40] W. Tomczak, The application of the nanofiltration membrane NF270 for separation of fermentation broths, Membranes 12 (12) (2022) 1263.
[41] O.P. Crossley, et al., Phosphorus recovery from process waste water made by the hydrothermal carbonisation of spent coffee grounds, Bioresour. Technol. 301 (2020) 122664.
[42] H. Lyu, et al., Monophenols separation from monosaccharides and acids by two-stage nanofiltration and reverse osmosis in hydrothermal liquefaction hydrolysates, J. Membr. Sci. 504 (2016) 141–152.
[43] Y. Du, et al., A mechanistic model for salt and water transport in leaky membranes: implications for low-salt-rejection reverse osmosis membranes, J. Membr. Sci. 678 (2023) 121642.
[44] D.F. Davidkova, et al., Influence of colloidal iron oxide and natural organic matter fouling on nanofiltration membrane performance: role of feed composition and membrane properties, Environ. Sci.:Water Res. Technol. 9 (11) (2023) 2942–2953.
[45] M. Gizińska-Górna, Z. Wasąg, Reliability and efficiency of the removal of pollutants in the mechanical–biological wastewater treatment plant A2/O, Desalination Water Treat. 246 (2022) 120–138.
[46] C. Fonseka, et al., Application of low-pressure nanofiltration membranes NF90 and NTR-729HF for treating diverse wastewater streams for irrigation use, Water 16 (14) (2024) 1971.
[47] Y.-L. Lin, N.-Y. Zheng, Y.-J. Hsu, Enhancing membrane separation performance in the conditions of different water electrical conductivity and fouling types via surface grafting modification of a nanofiltration membrane, NF90, Environ. Res. 239 (2023) 117346.
[48] A. Simon, et al., Effects of caustic cleaning on pore size of nanofiltration membranes and their rejection of trace organic chemicals, J. Membr. Sci. 447 (2013) 153–162.
[49] H. Laalaoua, et al., Surface characterization and interfacial analysis of organic membranes: an investigation on electrical and wettability phenomenon, Desalination Water Treat. 257 (2022) 34–40.
[50] Z. Qiu, et al., Enhancing rejection of endocrine disrupting compounds by nanofiltration membrane: dominant role of hydrophilic coordination barrier layer, Desalination 587 (2024) 117949.
[51] J. Huang, et al., New insights into effect of alkaline cleaning on fouling behavior of polyamide nanofiltration membrane for wastewater treatment, Sci. Total Environ. 780 (2021) 146632.
[52] B. Sutariya, S. Karan, A realistic approach for determining the pore size distribution of nanofiltration membranes, Sep. Purif. Technol. 293 (2022) 121096.
[53] H. Guo, et al., Does hydrophilic polydopamine coating enhance membrane rejection of hydrophobic endocrine-disrupting compounds? Environ. Sci. Technol. Lett. 3 (9) (2016) 332–338.
[54] U. Baig, et al., Facile modification of NF membrane by multi-layer deposition of polyelectrolytes for enhanced fouling resistance, Polymers 13 (21) (2021) 3728.
[55] R. Żyłła, et al., Impact of polymer membrane properties on the removal of pharmaceuticals, Membranes 12 (2) (2022) 150.
[56] J. Wang, et al., Fouling characteristics and cleaning strategies of NF membranes for the advanced treatment of antibiotic production wastewater, Environ. Sci. Pollut. Res. 24 (10) (2017) 8967–8977.
[57] P. Xu, C. Bellona, J.E. Drewes, Fouling of nanofiltration and reverse osmosis membranes during municipal wastewater reclamation: membrane autopsy results from pilot-scale investigations, J. Membr. Sci. 353 (1–2) (2010) 111–121.
[58] M. Al-Abri, et al., Autopsy of used reverse osmosis membranes from the largest seawater desalination plant in Oman, Membranes 12 (7) (2022) 671.
[59] Y.-L. Lin, et al., Mitigating silica fouling and improving PPCP removal by modified NF90 using in situ radical graft polymerization, Membranes 11 (11) (2021) 904.
[60] Y. Qi, et al., A novel nanofiltration membrane with simultaneously enhanced antifouling and antibacterial properties, RSC Adv. 9 (11) (2019) 6107–6117.
[61] J.V. Nicolini, C.P. Borges, H.C. Ferraz, Selective rejection of ions and correlation with surface properties of nanofiltration membranes, Sep. Purif. Technol. 171 (2016) 238–247.
[62] D. Park, et al., Impacts of monochloramine as an antifouling agent during nanofiltration (NF) of portable water, Desalination Water Treat. 180 (2020) 67–73.